Results in Physics 8 (2018) 621–627

Contents lists available at ScienceDirect

Results in Physics

journal homepage: www.journals.elsevier.com/results-in-physics

Hydromagnetic mixed convective flow over a wall with variable thickness and Cattaneo-Christov heat flux model: OHAM analysis

Muhammad Awais [a], Saeed Ehsan Awan [b], Khalid Iqbal [c], Zuhaib Ashfaq Khan [b], Muhammad Asif Zahoor Raja [b],*

[a] Dept. of Mathematics, COMSATS Institute of Information Technology, Attock Campus, Attock, Pakistan
[b] Dept. of Electrical Engineering, COMSATS Institute of Information Technology, Attock Campus, Attock, Pakistan
[c] Dept. of Computer Science, COMSATS Institute of Information Technology, Attock Campus, Attock, Pakistan

A R T I C L E   I N F O

Article history:
Received 1 November 2017
Received in revised form 14 December 2017
Accepted 15 December 2017
Available online 09 January 2018

Keywords:
Cattaneo-Christov heat flux model
OHAM analysis
Mixed convection
Internal heat generation/absorption

A B S T R A C T

The effect of Cattaneo-Christov heat flux model for the hydro-magnetic mixed convective flow of a non-Newtonian fluid is presented. The flow over a wall having variable thickness is anticipated under the influence of transverse magnetic field and internal heat generation/absorption effects. Mathematical formulation has been performed by making use of the suitable transformations. Convergence analysis has been performed and the optimal values are computed by employing optimal homotopy analysis method. The effects of physical parameters are elaborated in depth via graphical and numerical illustrations.
© 2017 The Authors. Published by Elsevier B.V. This is an open access article under the CC BY-NC-ND license (http://creativecommons.org/licenses/by-nc-nd/4.0/).

Introduction

Combining dynamic fluids with heat transfer is one of the useful topic due to its various technical and scientific applications. Recently it is acknowledged that the rate of cooling is significant in order to obtain the quality of the product. For-example in purification of molten metals, crystal growing and polymer processing, glass products, sheeting stuff (paper, fiber and metallic sheets), coating of wires etc. the rheology and rate of heat transfer have great importance. In view of these applications of heat transfer, several researchers [1–15] in the past have investigated different rheological problems with various technical and physical aspects including internally generated/absorbed heat, transfer of wall mass, hydrodynamics as well as hydro-magnetics, shrinking and stretching of boundaries, thermal-diffusion and diffusion-thermo effects etc. In studies [1–15], characteristics of transfer of heat are analyzed by considering the Fourier's law of heat conduction. However, Fourier's law is inadequate because of the fact of the initial disturbance that can be handled instantaneously throughout the system. Cattaneo [16] modified the Fourier's law by introducing the thermal relaxation time to overcome the observed difficulties. The thermal relation time addition permits the transportation of heat by propagating thermal waves with restricted speed. Christov [17] extended the work of Cattaneo by introducing the rate of change of Oldroyd's upper-convected factor for further investigation. Later on, several researchers and investigators extended this concept under various flow aspects. For-instance Tibullo and Zampoli [18] computed better results for the Cattaneo-Christov heat flux model (C-CHFM) can be applied to incompressible fluids. A validity analysis for the C-CHFM established a fact of a different solution for the problems of initial boundary values with an application to the incompressible flow of fluid. Thermal irregularity in Brinkman absorbent media with C-CHFM has been investigated by Haddad [19]. By employing the C-CHFM, significant factor for finding the convection instability threshold. The integrated flow and heat transfer in a viscoelastic fluid with C-CHFM has been proposed by Han et al. [20], in which authors have considered the upper-convected Maxwell fluid flow using slip boundary conditions and employed homotopy analysis method for computations and provide the comparative studies for Fourier law and C-CHFM. Hayat et al. [21] presented hydromagnetic flow of an Oldroyd-B fluid having mixed (similar/dissimilar) responses for the C-CHFM, and presented analysis through homotopy analysis method (HAM). Mustafa [22] presented C-CHFM for flow rotation with analysis of the heat transfer characteristic for an upper convected Maxwell (UCM) fluid model by exploiting both analytical and numerical approaches. In [23], a numerical study of

* Corresponding author.
E-mail addresses: awais@ciit-attock.edu.pk (M. Awais), saeed.ehsan@ciit-attock.edu.pk (S.E. Awan), khalid.iqbal@ciit-attock.edu.pk (K. Iqbal), zuhaibkhan@ciit-attock.edu.pk (Z.A. Khan), Muhammad.asif@ciit-attock.edu.pk (M.A.Z. Raja).

https://doi.org/10.1016/j.rinp.2017.12.043
2211-3797/© 2017 The Authors. Published by Elsevier B.V.
This is an open access article under the CC BY-NC-ND license (http://creativecommons.org/licenses/by-nc-nd/4.0/).

C-CHFM is presented with an aim to measure the effect of exponential surface stretch for viscoelastic flow using shooting method.

In this paper, we have extended the theory of C-CHFM. We have investigated the C-CHFM for the non-Newtonian fluid flow over a wall with variation in thickness. Influence of mixed convective phenomenon combined with the effects of magnetic field and internal heat generation/absorption are analyzed in detail. The best values of the convergence control parameters are presented in terms of graphical and numerical illustrations to study the emerging physical characteristics.

Problem formulation

We consider the hydro-magnetic mixed convective flow of an UCM fluid over a wall by variable thickness. The analysis of transferring heat has been investigated by using the C-CHFM and the internal heat generation/absorption effects are incorporated. According to the Cartesian system, along horizontal axis (x-axis) and vertical axis (y-axis) are taken along the stretching sheet and normal, respectively as shown in Fig. 1, while for the system, the boundary layer equations based on laws of mass, momentum and energy conservation is written in terms of PDEs as:

$$\frac{\partial u}{\partial v}+\frac{\partial v}{\partial y}=0, \tag{1}$$

$$\mathrm{u}\frac{\partial u}{\partial x}+v\frac{\partial u}{\partial y}=\nu\frac{\partial^2 u}{\partial y^2}-\lambda_1\left(u^2\frac{\partial^2 u}{\partial x^2}+v^2\frac{\partial^2 u}{\partial x^2}+2uv\frac{\partial^2 u}{\partial x\partial y}\right)-\frac{\sigma\beta_0^2}{\rho}\left(u+\lambda_1 v\frac{\partial u}{\partial y}\right)+g\beta_t(T-T_\infty), \tag{2}$$

$$\rho C_p \mathrm{v}\cdot\Delta\mathrm{T}=-\Delta\cdot\mathrm{q}, \tag{3}$$

where u and v are horizontal and vertical components of velocities, respectively. Whereas ν is stands for kinematic viscosity, T represents the fluid temperature, ρ is density of fluid, λ_1 is fluid relaxation time, q is heat flux, g is gravitational acceleration, B_0 is imposed magnetic field, Q_0 is heat generation absorption coefficient, T_∞ is ambient fluid temperature, T_w is condition at surface, σ is electric conductivity, β_t is volumetric expansion and C_p is the specific heat capacity. Moreover

$$q+\lambda_2\left(\frac{\partial q}{\partial t}+v\cdot\Delta q-q\cdot\Delta v+(\Delta\cdot v)q\right)=-K(\mathrm{T})\Delta T, \tag{4}$$

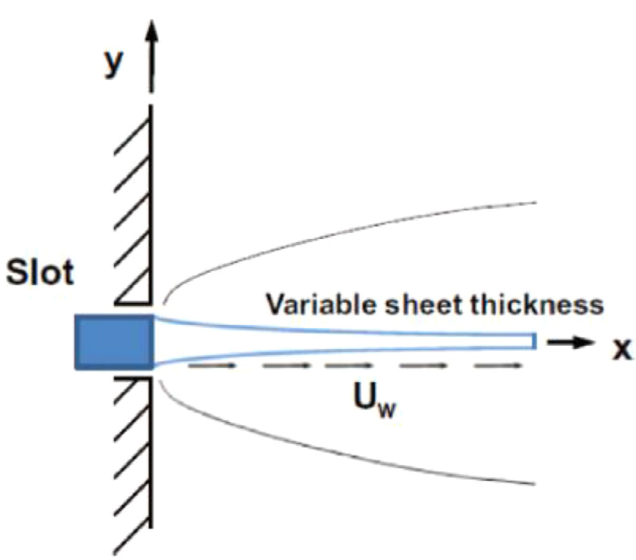

Fig. 1. Physical flow model.

In Eq. (4) λ_2 represents the thermal relaxation time, $K(T)$ is variable thermal conductivity. Simplifying Eqs. (3), (4), we get:

$$u\frac{\partial u}{\partial x}+v\frac{\partial T}{\partial y}=\lambda_2\left(u\frac{\partial u}{\partial x^2}\frac{\partial T}{\partial x}+v\frac{\partial v}{\partial y}\frac{\partial T}{\partial x}+u\frac{\partial v}{\partial x}\frac{\partial T}{\partial y}+v\frac{\partial v}{\partial y}\frac{\partial T}{\partial x}+2uv\frac{\partial^2 T}{\partial x\partial y}+u^2\frac{\partial^2 T}{\partial x^2}+v^2\frac{\partial^2 T}{\partial x^2}\right)=\frac{1}{\rho C_p}\frac{\partial}{\partial y}\left(K(\mathrm{T})\frac{\partial T}{\partial y}\right)+\frac{Q_0}{\rho C_p}(T-T_\infty)+\frac{Q_0\lambda_1}{\rho C_p}\left(u\frac{\partial T}{\partial x}+v\frac{\partial T}{\partial y}\right). \tag{5}$$

The boundary conditions in the present problems are:

$$u=u_w(x)=\mathrm{U}_0(x+b)^n,\quad \mathrm{v}=0,\quad \mathrm{T}=\mathrm{T}_w\quad at\ y=A(x+b)\frac{1-n}{2},$$
$$\mathrm{v}=0,\quad \mathrm{T}=\mathrm{T_w}\quad \text{at } y=A(x+b)\frac{1-n}{2},$$
$$u\to 0,\quad T\to T_\infty\quad as\ y\to\infty\quad T\to T_\infty,\quad \text{as } y\to\infty, \tag{6}$$

where $k(T)=k_\infty(1+\varepsilon\theta)$, k_∞ is the ambient thermal conductivity of the fluid, θ is the dimensionless temperature and ε is the small scalar parameter which shows the influence of temperature on variable thermal conductivity.

The following similarity transformations are invoked:

$$\psi=\sqrt{\frac{2}{n+1}\nu U_0(x+b)^{n+1}}F(\eta),$$
$$\eta=\sqrt{\frac{n+1}{2}\frac{U_0}{\nu}(x+b)^{n-1}}y,$$
$$u=U_0(x+b)^n F'(\eta),$$
$$v=-\sqrt{\frac{n+1}{2}\nu U_0(x+b)^{n-1}}\left[F(\eta)+\eta\frac{n-1}{n+1}F'(\eta)\right],\quad \theta(\eta)=\frac{T-T\infty}{T_w-T\infty}. \tag{7}$$

Making use of transformations given in Eq. (7), the Eqs. (1), (2) and (5) are written as:

$$F'''+FF''-\frac{2n}{1+n}F'^2+\beta\left(\begin{matrix}(3n+1)FF'F'''-\frac{2n(n-1)}{n+1}F'^3\\ +\eta\frac{n-1}{2}F'^2F''-\frac{n+1}{2}F^2F'''\end{matrix}\right)-M\left(\frac{2}{n+1}F'-\beta FF''-\eta\beta\frac{n-1}{n+1}F'F''\right)+\lambda\left(\frac{2}{n+1}\theta\right)=0 \tag{8}$$

$$(1+\varepsilon\Theta)\Theta''+\varepsilon\Theta'^2+\Pr\left(\begin{matrix}\gamma\left(\frac{n-3}{2}FF'\Theta'-\frac{n+1}{2}F^2\Theta''\right)\\ +F\Theta'+h_s\left(\frac{2}{n+1}\Theta\right)-h_s\gamma F\Theta'\end{matrix}\right)=0, \tag{9}$$

and the boundary conditions become

$$F(\alpha)=\alpha\frac{(1-n)}{(1+n)},\quad F'(\alpha)=1,\quad \Theta(\alpha)=1,\quad \Theta(\infty)\to 0, \tag{10}$$

where $\alpha=A\sqrt{\frac{n+1}{2}\frac{U_0}{\nu}}$ describes the plate surface. We define $F(\eta)=f(\eta-\alpha)=f(\xi)$ so that the above equation yield:

$$f'''+ff''-\frac{2n}{1+n}f'^2+\beta\left(\begin{matrix}(3n+1)ff'f''-\frac{2n(n-1)}{n+1}f'^3\\ +\eta\frac{n-1}{2}f'^2f''-\frac{n+1}{2}f^2f'''\end{matrix}\right)-M\left(\frac{2}{n+1}f'-\beta ff''-\eta\beta\frac{n-1}{n+1}f'f''\right)+\lambda\left(\frac{2}{n+1}\theta\right)=0 \tag{11}$$

$$(1+\varepsilon\theta)\theta''+\varepsilon\theta'^2+\Pr\left(\begin{matrix}\gamma\left(\frac{n-3}{2}ff'\theta'-\frac{n+1}{2}\theta''f^2\right)\\ +f\theta'+h_s\left(\frac{2}{n+1}\theta\right)-h_s\gamma f\theta'\end{matrix}\right)=0, \tag{12}$$

and

$$f(0) = \alpha\frac{(1-n)}{(1+n)}, \quad f'(0) = \theta(0) = 1, \quad f'(\infty) \to 0, \quad \theta(\infty) = 0, \tag{13}$$

where h_s, M, λ and γ are the heat source/sink, magnetic, and the mixed convection parameters, respectively, while, Pr and β is Prandtl and Deborah number in terms of relaxation time, respectively. These quantities are defined mathematically as follows:

$$M = \frac{\sigma B_0^2}{\rho U_0 (x+b)^{n-1}}, \quad h_s = \frac{Q_0}{\rho C_p U_0 (x+b)^{n-1}}, \quad \lambda = \frac{g\beta_t (T_w - T_\infty)}{U_0^2 (x+b)^{2n-1}},$$
$$\Pr = \frac{\mu C_p}{k_\infty}, \quad \beta = \lambda_1 U_0 (x+b)^{n-1}, \quad \gamma = \lambda_2 U_0 (x+b)^{n-1}, \tag{14}$$

Solution methodology

It is noted that the Eqs. (11) and (12) along with boundary conditions (13) are the two non-linear ordinary differential equations (ODEs). With the aim of computing the solutions, the HAM is employed, while the optimal values are determined using optimal HAM (OHAM). By defining the initial guess for both (f_0, θ_0) and (L_f, L_θ) as:

$$f_0(\eta) = \alpha\frac{1-n}{1+n} + 1 - \exp(-\eta), \quad \theta_0(\eta) = \exp(-\eta), \tag{15}$$

$$L_f(f) = \frac{d^3 f}{d\eta^3} - \frac{df}{d\eta}, \quad L_\theta(\theta) = \frac{d^2 f}{d\eta^2} - \theta, \tag{16}$$

The problems at the zeroth order deformation are

$$L_f[f^\wedge(\eta,p) - f_0(\eta)] - \frac{p}{(1-p)} h_f [f^\wedge(\eta,p)] = 0, \tag{17}$$

$$L_\theta[\theta^\wedge(\eta,p) - \theta_0(\eta)] - \frac{p}{(1-p)} h_\theta N_\theta[\theta^\wedge(\eta,p), f^\wedge(\eta,p)] = 0, \tag{18}$$

$$f^\wedge(0;p) - \alpha\frac{(1-n)}{(1+n)} = 0, \quad f^\wedge(0;p) = \theta^\wedge(0;p) = 1, \quad f^{\wedge\prime}(\infty;p) \to 0,$$
$$\theta^\wedge(\infty;p) \to 0, \tag{19}$$

where the nonlinear operators are given by

$$\begin{aligned} N_f = [f^\wedge(\eta;p)] &= \frac{\partial^3 f^\wedge(\eta;p)}{\partial\eta^3} + (3n-1) f^\wedge(\eta;p)\frac{\partial f^\wedge(\eta;p)}{\partial\eta}\frac{\partial^2 f^\wedge}{\partial\eta^2} \\ &- \frac{2n(n-1)}{n+1}\left(\frac{\partial f^\wedge(\eta;p)}{\partial\eta}\right)^3 + f^{\wedge 2}(\eta;p)\frac{\partial^2 f^\wedge(\eta;p)}{\partial\eta^2} \\ &- M\begin{pmatrix} \frac{2}{n+1} f^\wedge(\eta;p) - \beta f^\wedge(\eta;p)\frac{\partial^2 f^\wedge(\eta;p)}{\partial\eta^2} \\ -\eta\beta\frac{n-1}{n+1}\frac{\partial f^\wedge(\eta;p)}{\partial\eta}\frac{\partial^2 f^\wedge(\eta;p)}{\partial\eta^2} \end{pmatrix} + \lambda\left(\frac{2}{n+1}\theta^\wedge(\eta;p)\right) \\ &+ \eta\frac{n-1}{2}\left(\frac{\partial(f^\wedge;p)}{\partial\eta}\right)^2\frac{\partial^2 f^\wedge(\eta;p)}{\partial\eta^2} - \frac{n+1}{2} f^{\wedge 2}(\eta;p)\frac{\partial^3 f^\wedge(\eta;p)}{\partial\eta^3} \\ &- \frac{2n}{n+1}\left(\frac{\partial f^\wedge(\eta;p)}{\partial\eta}\right)^2 \end{aligned} \tag{20}$$

$$\begin{aligned} N_\theta = [\theta^\wedge(\eta;p)] &= (1 + \varepsilon\theta^\wedge(\eta;p))\frac{\partial^2\theta^\wedge(\eta;p)}{\partial\eta^2} + \varepsilon\left(\frac{\partial\theta^\wedge(\eta;p)}{\partial\eta}\right)^2 \\ &+ \Pr f^\wedge(\eta;p)\frac{\partial\theta^\wedge(\eta;p)}{\partial\eta} + \Pr\left(\gamma\begin{pmatrix} \frac{n-3}{2} f^\wedge(\eta;p)\frac{\partial f^\wedge(\eta;p)}{\partial\eta}\frac{\partial\theta^\wedge}{\partial\eta} \\ -\frac{n+1}{2}\left(\frac{\partial(f^\wedge;p)}{\partial\eta}\right)^2\frac{\partial^2\theta^\wedge(\eta;p)}{\partial\eta^2} \end{pmatrix}\right. \\ &\left.+ h_s\begin{pmatrix} \left(\frac{2}{n+1}\theta^\wedge(\eta;p)\right) \\ -\gamma f^\wedge(\eta;p)\frac{\partial\theta^\wedge(\eta;p)}{\partial\eta} \end{pmatrix}\right), \end{aligned} \tag{21}$$

Whereas the mth order problems are

$$L_f[f_m(\eta) - X_m f_{n-1}(\eta)] = h_f R_m^f(\eta), \tag{22}$$

$$L_\theta[\theta_m(\eta) - X_m \theta_{m-1}(\eta)] = h_\theta R_m^\theta(\eta), \tag{23}$$

$$f_m(0) = 0, \quad f'_m(0) = 0, \quad f_m(\infty) = 0, \quad \theta_m(0) = 0, \quad \theta_m(\infty) = 0, \tag{24}$$

$$\begin{aligned} R_m^f(\eta) &= f'''_{m-1}(\eta) + \sum_{k=0}^{m-1}\left(f_{m-1-k}(\eta) f''_k - \frac{2n}{1+n} f'_{m-1-k} f'_k\right) \\ &+ \lambda\frac{2}{n+1}\theta_{m-1} \\ &+ \beta\left(\sum_{k=0}^{m-1} f'_{m-1-k}\sum_{l=0}^{k}((3n-1) f'_{k-l} f''_l - \frac{n+1}{2} f_{k-l} f'''_l)\right) \\ &+ \beta\left(f'_{m-1-k}\sum_{l=0}^{k}(\eta\frac{(n-1)}{2} f'_{k-l} f''_l - \frac{2n(n-1)}{n+1} f'_{k-l} f'_l)\right) \\ &- M\left(\frac{2}{n+1} f'_{m-1} - \sum_{k=0}^{m-1}(f_{m-1-k} f''_k - \eta\beta\frac{n-1}{n+1} f'_{m-1-k} f''_k)\right) \end{aligned} \tag{25}$$

$$\begin{aligned} R_m^\theta(\eta) &= \theta'''_{m-1}(\eta) + \varepsilon\sum_{k=0}^{m-1}\left(\theta_{m-l-k}(\eta)\theta''_k + \varepsilon\sum_{k=0}^{m-1}\theta'_{m-1-k}\theta'_k\right) \\ &+ \beta\left(\sum_{k=0}^{m-1} f'_{m-1-k} + \Pr\sum_{k=0}^{m-1} f_{m-1-k}\theta'_k\right) \\ &+ \Pr\begin{pmatrix} \gamma\sum_{k=0}^{m-1}\left(f_{m-1-k}\sum_{l=0}^{k}\left(\frac{n-3}{2} f'_{k-l}\theta'_l - \frac{n+1}{2} f_{k-1}\theta''_l\right)\right) \\ + h_s\frac{2}{n+1}\theta_{m-1} - h_s\gamma\sum_{k=0}^{m-1} f_{m-1-k}\theta'_k \end{pmatrix} \end{aligned} \tag{26}$$

and the chi function is defined as

$$\begin{aligned} X_m &= 0, \quad \text{when } m \leqslant 1, \\ X_m &= 1, \quad \text{when } m > 1, \end{aligned} \tag{27}$$

It is noted that for $p = 0$ and $p = 1$, we can write:

$$f^\wedge(\eta;0) = f_0(\eta), \quad f^\wedge(\eta;1) = f(\eta;1) = f(\eta), \tag{28}$$

$$\theta^\wedge(\eta;0) = \theta_0(\eta), \quad \theta^\wedge(\eta;1) = \theta(\eta), \tag{29}$$

We take $p \in [0,1]$, from the said variation $f^\wedge(\eta;1)$ and $\theta^\wedge(\eta;p)$ from the initial solution $f_0(\eta)$ and $\theta_0(\eta)$ to the final solution $f(\eta)$ and $\theta(\eta)$. By exploiting the Taylor series expansion, we get

$$f(\eta;p) = f_0(\eta) + \sum_{m=1}^{\infty} f_m(\eta) p^m, \quad f_m(\eta) = \frac{1}{m!}\frac{\partial^m f(\eta;p)}{\partial p^m}\bigg|_{p=0}, \tag{30}$$

$$\theta(\eta;p) = \theta_0(\eta) + \sum_{m=1}^{\infty}\theta_m(\eta) p^m, \quad \theta_m(\eta) = \frac{1}{m!}\frac{\partial^m\theta(\eta;p)}{\partial p^m}\bigg|_{p=0}, \tag{31}$$

We chose the auxiliary parameter in such a means that the above expression (30) and (31) transformed at point $p = 1$ as

$$f(\eta) = f_0(\eta) + \sum_{m=1}^{\infty} f_m(\eta), \tag{32}$$

$$\theta(\eta) = \theta_0(\eta) + \sum_{m=1}^{\infty}\theta_m(\eta), \tag{33}$$

Optimal analysis

Since homotopic series results conventionally covers the non-zero auxiliary factors c_0^f and c_0^θ that state the convergence-region of the Homotopy series solutions. To get optimal values of c_0^f and c_0^θ parameters, the optimal analysis through minimization process is utilized for average squared residual errors as follows:

$$E_m^f = \frac{1}{k+1}\sum_{j=0}^{k}\left(N_f\left(\sum_{i=0}^{m}\hat{f}(\eta),\ \sum_{i=0}^{m}\hat{\theta}(\eta)\right)_{\eta=j\delta\eta}\right)^2 dn, \tag{34}$$

$$E_m^\theta = \frac{1}{k+1}\sum_{j=0}^{k}\left(N_\theta\left(\sum_{i=0}^{m}\hat{f}(\eta),\ \sum_{i=0}^{m}\theta(\eta)\right)_{\eta=j\delta\eta}\right)^2 dn \tag{35}$$

$$E_m^t = E_m^f + E_m^\theta, \tag{36}$$

where E_m^t is the sum of both residual errors, while $\delta\eta = 0.5$ and $k = 20$ are taken.

The obtained minimum magnitude of E_m^t for a set of control global optimal gauges for different approximation orders are presented in Table 1. Four set of control global optimal gauges at 2, 4, 6 and 8th approximation orders are determined. The values of E_m^f, and E_m^θ errors are listed in Table 2 and Figs. 2 and 3 at different order of approximations using 8th order control global optimal gauge. It is observed that the magnitudes of errors, i.e., E_m^f, and E_m^θ decreased with an increase in the order of approximations.

Discussion

The goal of this portion is to present the effects of involved physical and rheological quantities. Therefore, we have plotted Figs. 4–13 which present the effects of Deborah number, magnetic field, mixed convection parameter, index number, thermal relaxation parameter and internal heat generation/absorption quantities. Fig. 4 presents the 3D flow configuration of the considered analysis. The velocity of the fluid strongly depends upon the initial velocity of the wall can be noted. Fig. 5 illustrates the effects of Deborah number β on velocity profile f'. It is noted that Deborah numbers retards the flow. It is because domain of β presents the difference between the solid state and liquid state. It is noted that any material behaves like liquid for small Deborah numbers whereas for higher values of Deborah number, material show viscoelastic nature. This nature is also observed in current analysis. Fig. 6 elucidates the effects of magnetic field on the fluids' velocity. It is observed that with an increase in magnetic field, the velocity of the fluid and the momentum boundary layer show decreasing behavior. From this result, we can say that the fluid velocity can be controlled by applying the magnetic field. The impacts of mixed convection parameter λ on the velocity profile f' are portrayed in Figs. 7 and 8. It is seen that the effects of increasing values of mixed convection parameter retards the velocity profile. Physically $\lambda \leqslant 0$ represents the internal cooling and $\lambda \geqslant 0$ meaning internal heating

Table 1
Best convergence control factors along with magnitude of the residual errors using **BVPH2.0.**

m	c_0^f	c_0^θ	E_m^t	CPU TIME [S]
2.0	−1.58	−1.37	4.32×10^{-5}	2.93
4.0	−1.45	−1.31	1.71×10^{-6}	55.12
6.0	−1.41	−1.27	2.94×10^{-7}	3120.98
8.0	−1.38	−1.23	0.52×10^{-7}	5141.54

Table 2
Magnitudes of error with optimal parameter $m = 8$ from Table 1.

m	E_m^f	E_m^θ	CPU TIME [S]
4.0	8.12×10^{-6}	9.68×10^{-7}	10.81
8.0	5.95×10^{-8}	3.61×10^{-9}	105.89
12.0	8.170×10^{-10}	9.41×10^{-11}	298.54

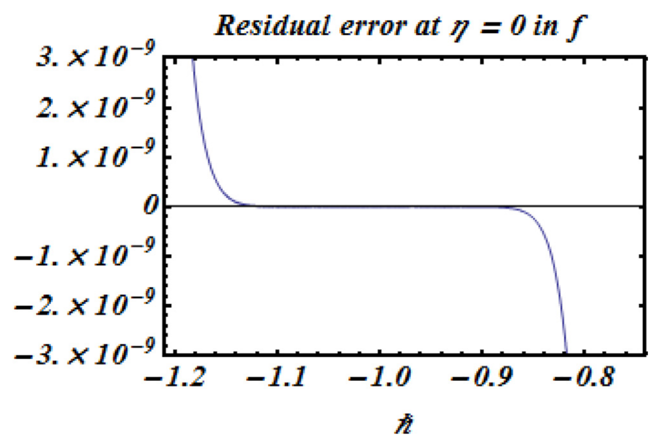

Fig. 2. Magnitude of error for f.

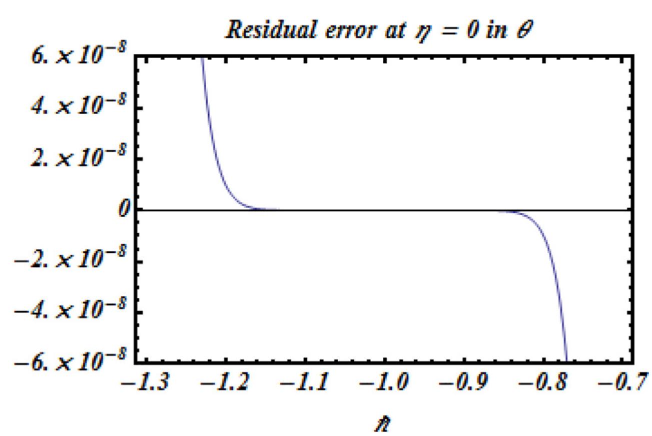

Fig. 3. Magnitude of error for θ.

whereas $\lambda = 0$ means absence of free convection current. The effect of decreasing value of mixed convection parameter $\lambda \leqslant 0$ on velocity profile results into a decrease in the fluids' velocity whereas for $\lambda > 0$, the fluid velocity increases. Therefore, we can conclude the mixed convection has opposite behavior for internal cooling and internal heating processes. Effects of power index number n on velocity profile are described in Fig. 9. It is noted that higher the value of power index number n result is increase in velocity profile. Since the wall motion is strongly dependent on power index n and an increase in n corresponds to an increase in the wall motion which induced the flow. Therefore, we conclude that by increase the value of power index n, one can enhance the fluids velocity. The behavior of thermal relaxation parameter γ on the temperature is showed in Fig. 10. It is noted that the higher value of thermal relaxation parameter γ results in reduction in temperature. In others words we can say that if increase the value of thermal relaxation parameter γ, then it shows a non-conducting behavior. It is also noted that the temperature distribution can be increased only for $\gamma = 0$, otherwise for the higher value of γ, the reduction in temperature is noted. Figs. 11 and 12 illustrate the effects of heat source parameter $(hs > 0)$ and heat sink

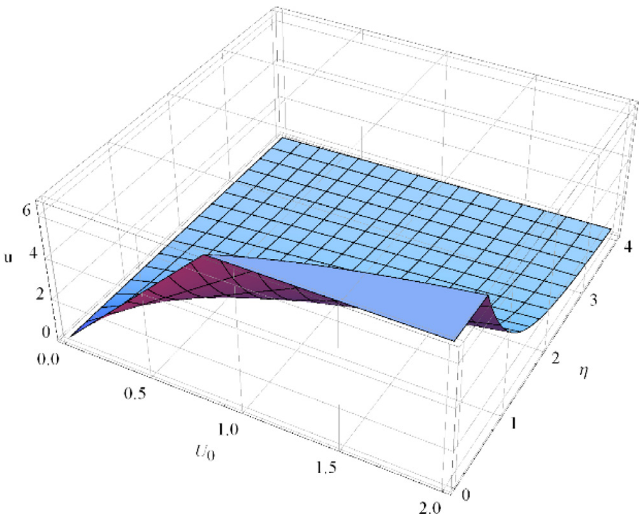

Fig. 4. 3D flow configuration.

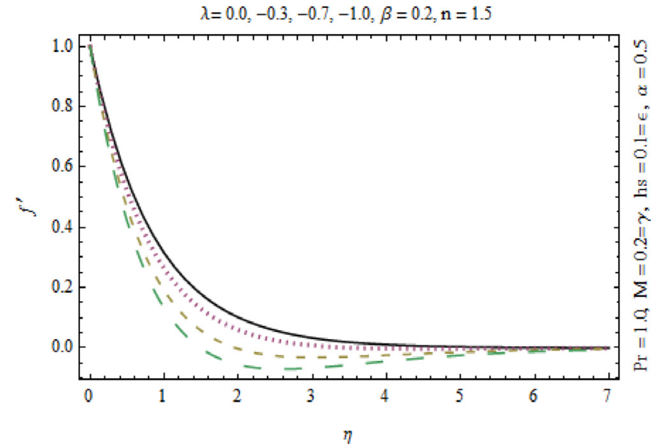

Fig. 7. Effects of $\lambda < 0$ on f'.

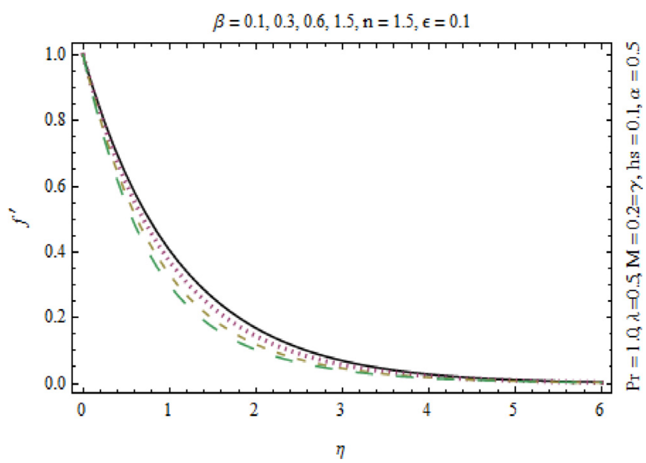

Fig. 5. Effects of β on f'.

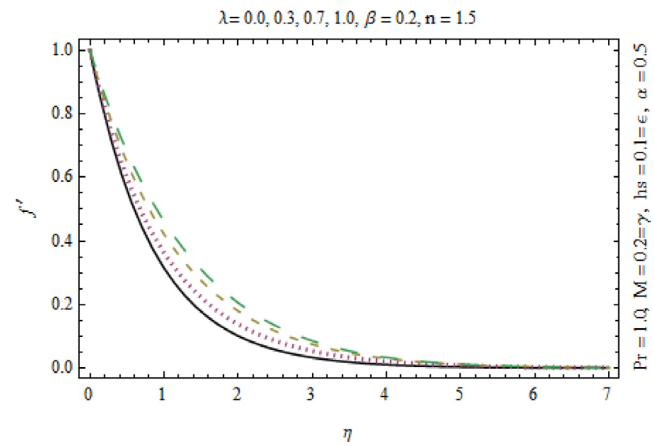

Fig. 8. Effects of $\lambda > 0$ on f'.

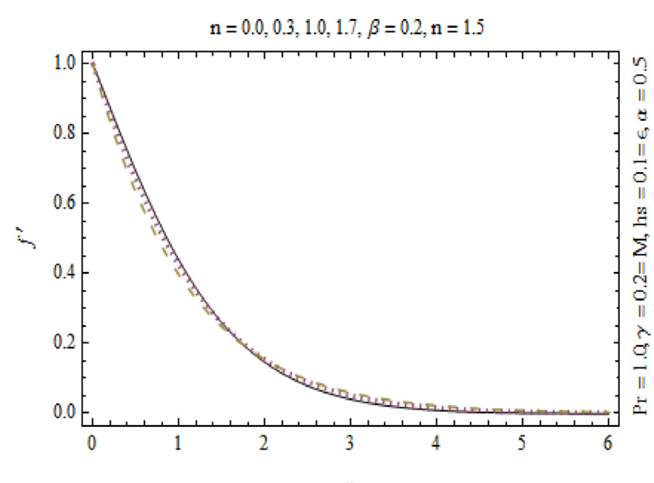

Fig. 9. Effects of n on f'.

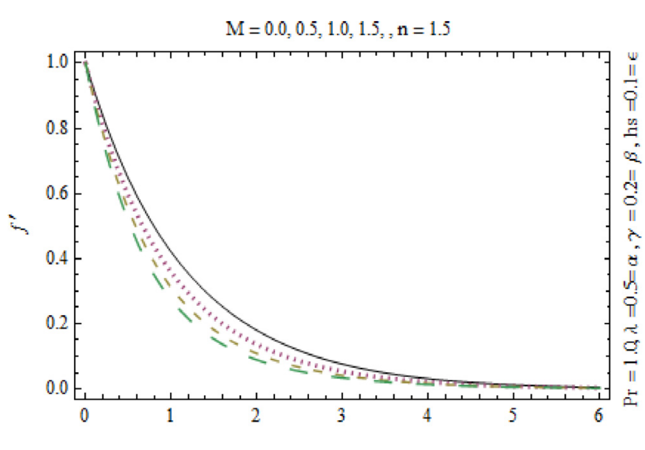

Fig. 6. Effects of M on f'.

parameter (hs < 0) on temperature profile θ. We have observed that the temperature of the fluid show increasing behavior for larger positive values of heat source whereas the temperature decreases with an increase in heat sink quantity. Moreover, the change in temperature for the case of heat source is significant when compared with the case when heat sink. The effects of mixed convection parameter λ on the temperature profile is presented in Fig. 13. It is noted that temperature decreases with an increase in the mixed convection parameter.

Complexity comparison of the numerical solvers is also conducted for the system model on the similar procedure as adopted

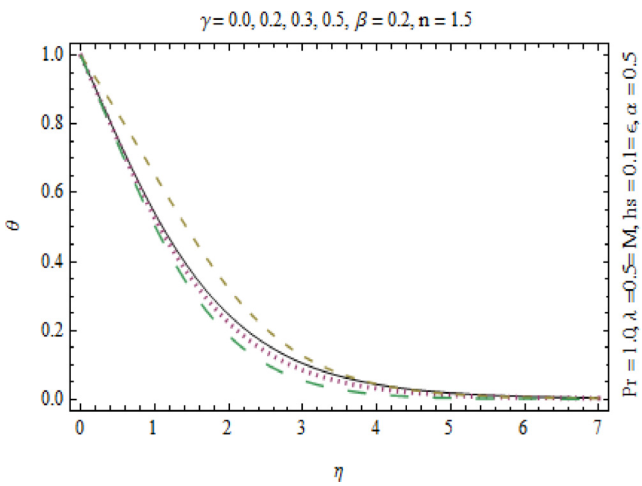

Fig. 10. Effects of γ on θ.

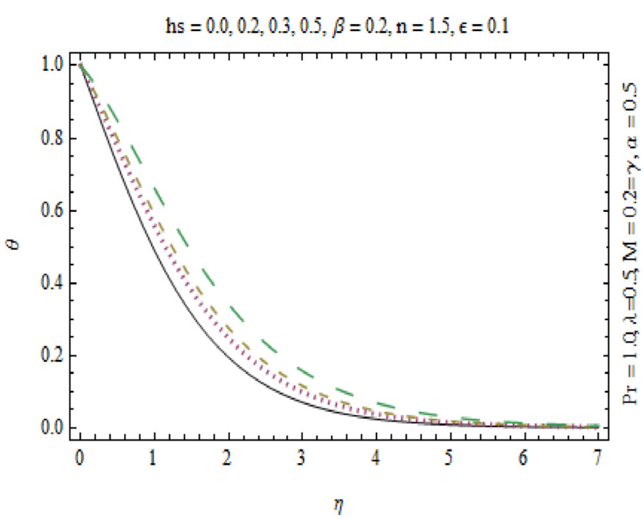

Fig. 11. Effects of $hs > 0$ on θ.

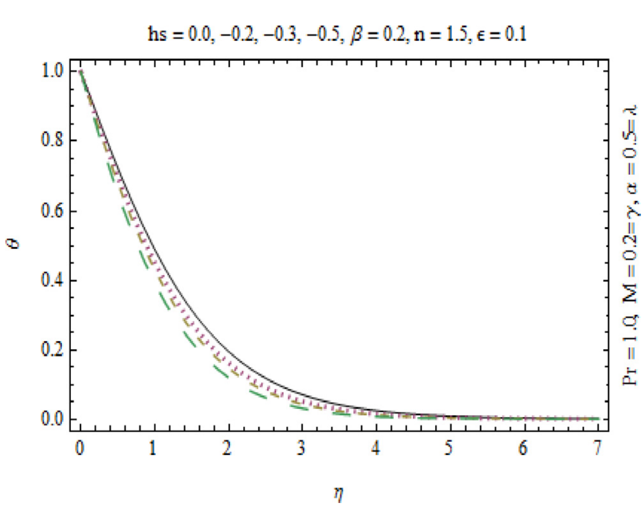

Fig. 12. Effects of $hs < 0$ on θ.

in [24–30] and result are given in terms of time consumed, number of step performed and number of function evaluated in Table 3. It is found that Adam numerical procedure will take the least time,

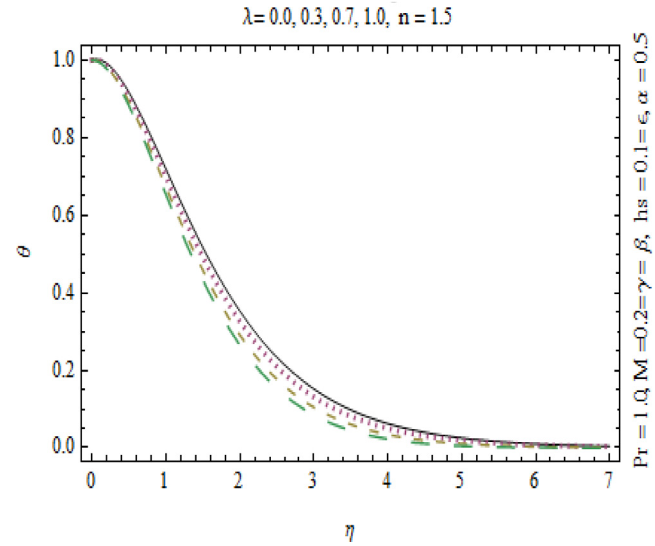

Fig. 13. Effects of λ on θ.

Table 3
Computation complexity of the solvers.

Method	Timing	Steps	Evaluations
Automatic	0.15625	36	75
Adams	0.1250	36	75
BDF	453,125	54	69
Explicit Runge Kutta	0.3125	11	179
Implicit Runge Kutta	1.296875	23	327
Extrapolation	0.59375	12	246

while Explicit Runge Kutta have performed with minimum steps and least function evaluations are consumed by BDF method.

Final outcomes

Following are some main outcomes of the considered analysis:

- Higher value of β, i.e., Deborah number, resultantly we observe the reduction in the velocity and momentum boundary layer thickness.
- Effect of mixed convection parameter has dual effects on the momentum and thermal boundary layers.
- Hydro-dynamics can be utilized in order to control the fluid flow and internal molecular movement.
- Increase in thermal relaxation time results into decrease in temperature.

Presence of heat sink decreases the temperature whereas heat source enhances the fluid temperature.

References

[1] Fetecau C, Vieru D, Fetecau C, Akhter A. General solutions for the magneto-hydrodynamic natural convection flow with radiative heat transfer and slip conditions over a moving plate. Z Naturforsch 2013;68(a):659–67.
[2] Mehmood O, Fetecau C. A note on radiative heat transfer to peristaltic flow of Sisko fluid. Appl Bionics Biomech 2015;2015(283892).
[3] Iqbal Z, Qasim M, Awais M, Hayat T, Asghar S. Stagnation-point flow by an exponentially stretching sheet in the presence of viscous dissipation and thermal radiation. J Aerosp Eng 2016;29(2).
[4] Ellahi R, Ariel PD, Hayat T, Asghar S. Effects of heat transfer on a third grade fluid in a flat channel. Int J Numer Methods Fluids 2010;63:847–50.
[5] Ellahi R. The effects of MHD and temperature dependent viscosity on the flow of non-Newtonian nanofluid in a pipe: analytical solutions. Appl Math Mod 2013;37:1451–67.

[6] Sheikholeslami M, Ashorynejad HR, Ganji DD, Rashidi MM. Heat and mass transfer of a micropolar fluid in a porous channel. Commun Numer Anal 2014;2014(2). can-00166.
[7] Sheikholeslami M, Hatami M, Ganji DD. Micropolar fluid flow and heat transfer in a permeable channel using analytical method. J Mol Liq 2014;194:30–6.
[8] Awais M, Hayat T, Nawaz M, Alsaedi A. Newtonian heating, thermal-diffusion and diffusion-thermo effects in an axisymmetric flow of a Jeffery fluid over a stretching surface. Braz J Chem Eng 2015;32:555–61.
[9] Rashidi MM, Rostami B, Freidoonimehr N, Abbasbandy S. Free convection heat and mass transfer for MHD fluid flow over a permeable vertical stretching sheet in the presence of radiation and buoyancy effects. Ain Shams Eng J 2014;6:901–12.
[10] Rashidi MM, Kayyani N, Abelman S. Investigation of entropy generation in MHD and slip flow over a rotating porous disk with variable properties. Int J Heat Mass Transfer 2014;70:892–917.
[11] Saleem M, Awais M, Nadeem S, Sandeep N, Mustafa T. Theoretical analysis of upper-convected Maxwell fluid flow with Cattaneo-Christov heat flux model. Chin J Phys 2017. https://doi.org/10.1016/j.cjph.2017.04.005.
[12] Hayat T, Muhammad T, Alsaedi A, Ahmad B. Three-dimensional flow of nanofluid with Cattaneo-Christov double diffusion. Results Phys 2016;6:897–903.
[13] Hatami M, Safari H. Effect of inside heated cylinder on the natural convection heat transfer of nanofluids in a wavy-wall enclosure. Int J Heat Mass Transfer 2016;103:1053–7.
[14] Hatami M, Khazayinejad M, Jing D. Forced convection of Al2O3–water nanofluid flow over a porous plate under the variable magnetic field effect. Int J Heat Mass Transfer 2016;102:622–30.
[15] Hatami M, Song D, Jing D. Optimization of a circular-wavy cavity filled by nanofluid under the natural convection heat transfer condition. Int J Heat Mass Transfer 2016;98:758–67.
[16] Cattaneo C. Sulla Conduzione del calore. Atti Semin Mat Fis Univ Modea Reggio Emilia 1948;3:83–101.
[17] Hayat T, Aziz A, Muhammad T, Alsaedi A. Model and comparative study for flow of viscoelastic nanofluids with Cattaneo-Christov double diffusion. PLoS One 2017. https://doi.org/10.1371/journal.pone.0168824.
[18] Tibullo V, Zampoli V. A uniquemess result for the Cattaneo-Christov heat conduction model applied to incompressible fluids. Mech Res Commun 2011;38:77–9.
[19] Haddad SAM. Thermal instability in Brinkman porous media with Cattaneo-Christov heat flux. Int J Heat Mass Transfer 2014;68:659–68.
[20] Han S, Zheng L, Li C, Zhang X. Coupled flow and heat transfer in viscoelastic fluids with Cattaneo-Christov heat flux model. Appl Math Lett 2014;38:87–93.
[21] Hayat T, Imtiaz M, Alsaedi A, Almezal S. On Cattaneo-Christov heat flux in MHD flow of Oldroyd-B fluid with homogeneous-heterogeneous reactions. J Magn Magn Mater 2016;401:296–303.
[22] Mustafa M. Cattaneo-Christov heat flux model for rotating flow and heat transfer of upper-convected Maxwell fluid. AIP Adv 2015;5:047109.
[23] Khan JA, Mustafa M, Hayat T, Alsaedi A. Numerical study of Cattaneo-Christov heat flux model for viscoelastic flow due to an exponentially stretching surface. PLoS One 2015;10(e0137363).
[24] Khan JA, Raja MAZ, Rashidi MM, Syam MI, Wazwaz AM. Nature-inspired computing approach for solving non-linear singular Emden–Fowler problem arising in electromagnetic theory. Connection Sci 2015;27(04):377–96. https://doi.org/10.1080/09540091.2015.1092499.
[25] Raja MAZ, Ahmad I, Khan I, Syam MI, Wazwaz AM. Neuro-heuristic computational intelligence for solving nonlinear pantograph systems. Front Inf Technol Electron Eng 2017;18(4):464–84.
[26] Raja MAZ, Shah FH, Syam MI. Intelligent computing approach to solve the nonlinear Van der Pol system for heartbeat model. Neural Comput Appl 2017:1–25.
[27] Raja MAZ, Abbas S, Syam MI, Wazwaz AM. Design of neuro-evolutionary model for solving nonlinear singularly perturbed boundary value problems. Appl Soft Comput 2018;62:373–94.
[28] Raja MAZ, Manzar MA, Shah FH, Shah FH. Intelligent computing for Mathieu's systems for parameter excitation, vertically driven pendulum and dusty plasma models. Appl Soft Comput 2018;62:359–72.
[29] Raja MAZ, Ahmed T, Shah SM. Intelligent computing strategy to analyze the dynamics of convective heat transfer in MHD slip flow over stretching surface involving carbon nanotubes. J Taiwan Inst Chem Eng 2017;80:935–53.
[30] Khan JA, Raja MAZ, Syam MI, Tanoli SAK, Awan SE. Design and application of nature inspired computing approach for non-linear stiff oscillatory problems. Neural Comput Appl 2015;26(7):1763–80. https://doi.org/10.1007/s00521-015-1841-z.